EGU 2022

Analysis of pan-tropical GNSS-R observations from CYGNSS satellites for floods detection and mapping

Pierre ZEIGER*, Frédéric FRAPPART, José DARROZES

** LEGOS, Observatoire Midi-Pyrénées, Université Paul Sabatier, Toulouse, France*

Contents

GNSS signals of opportunity

Bistatic Radar → Information about the reflecting surface

→ L-band signals (λ_{L1} = 19.03 cm)
→ Correlation of the reflected signal with a replica of the direct signal
→ Observable: Delay Doppler Maps (DDMs)

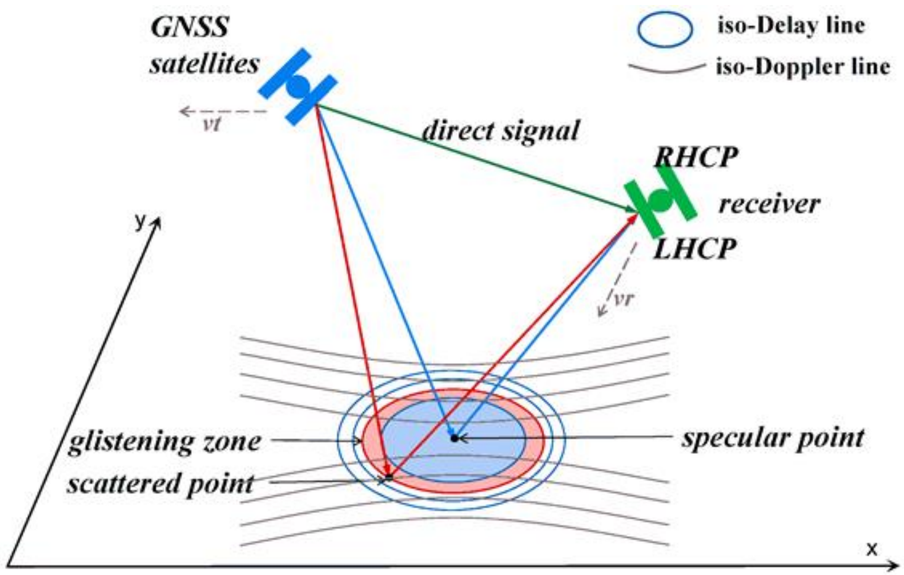

Examples of DDM

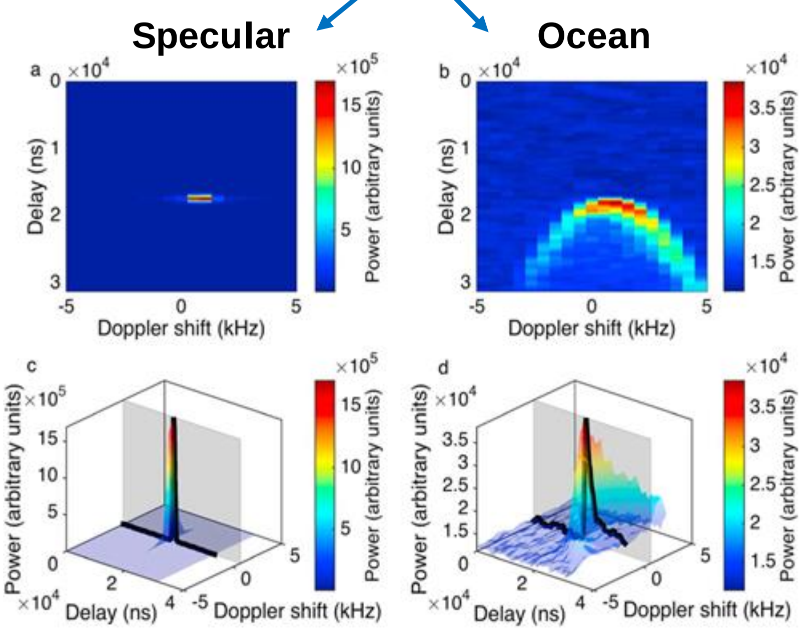

Chew et al. (2016)

The CYGNSS mission

- **Spatial resolution**
  - → Fresnel area ~ 0.6 to 1 km (**coherent scattering)**
  - → Incoherent integration of the reflected signals (1s)
  - → Spatial resolution ~ 1 x 7 km (**over land)**
    ~ 25 km (**over ocean**)
  - → **Inter-tropical band only** (+- 38° lat)

- **Multi-incidence measurements**
  - → Incidence from 0 to >70°

- **8 instruments able to track 4 GNSS satellites each**
  - → 32 observations / second
  - → Satellite overpass ~1.5 hrs
  - → pseudo-random repartition (bistatic configuration)
  - → Temporal resolution ~ 1-2 days over ocean (**incoherent scattering**)

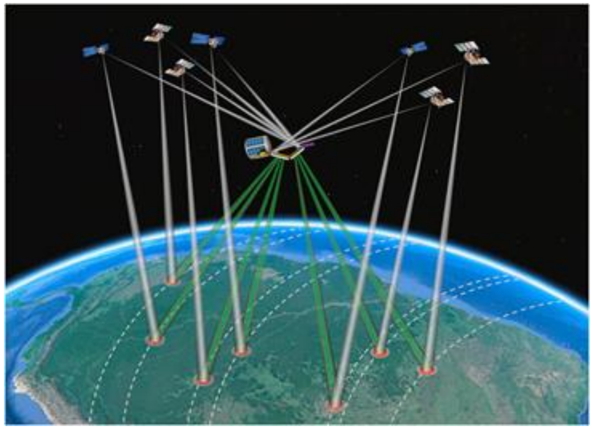

Nghiem et al., 2016

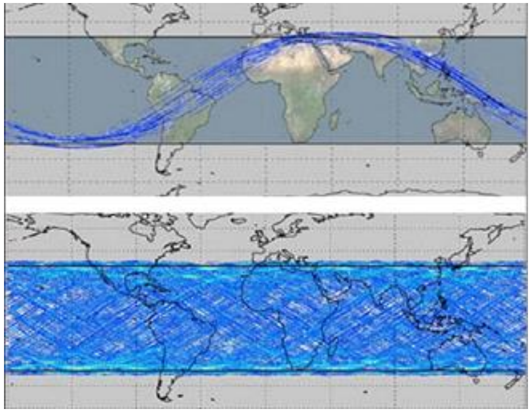

Source : NASA

Applications of spaceborne GNSS-R

GNSS-R
Zavorotny et al., 2014 (tutorial)
CYGNSS
Ruf et al., 2016

Wind speed
Clarizia et al., 2016
Ruf et al., 2018

Vegetation
Jensen et al., 2018

Soil moisture
Chew & Small, 2018a
Clarizia et al., 2019
Eroglu et al., 2019
Yan et al., 2020

Floods
Chew et al., 2018b
Jensen et al., 2018
Morris et al., 2019
Rodriguez-Alvarez et al., 2019

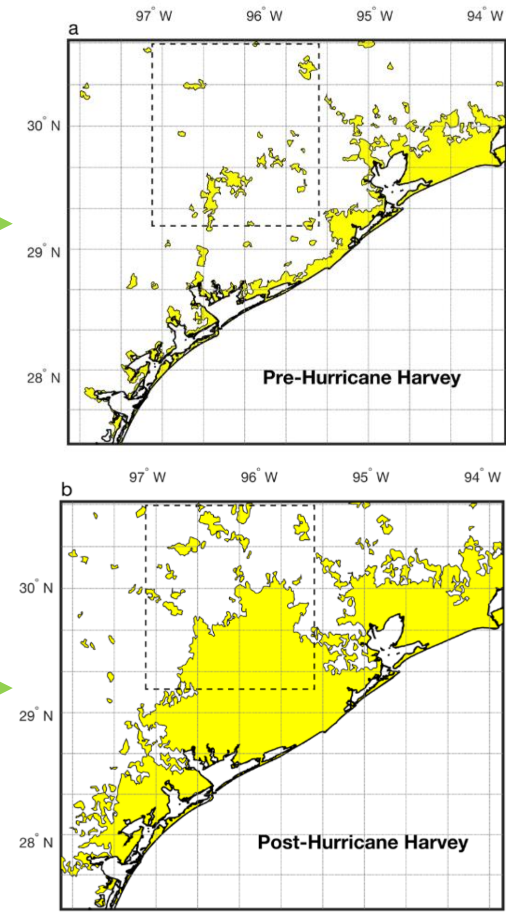

Inundated areas before and after hurricane Harvey in Texas, 2017. From Chew & Small, 2018b

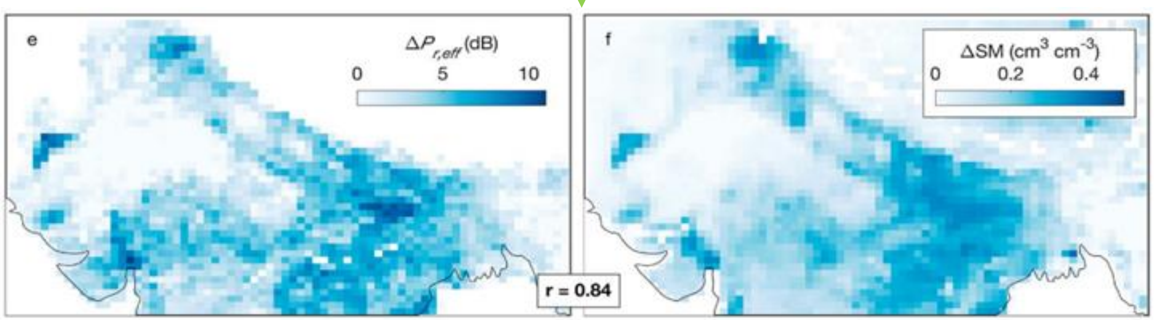

Maps of the change in CYGNSS power and SM content. From Chew & Small, 2018a

Monitoring of flood dynamics

	Limitations
➢ **At the global scale** → Using active and passive microwave instruments, *i.e.* **GIEMS** (*Prigent et al., 2020*), **SWAMPS** (*Jensen et al., 2019*)	Coarse spatial (0.25°) and temporal (1-month) resolutions
→ Using multispectral imagery like Landsat (*Pekel et al., 2016)*	No data over vegetated areas, mask with cloud cover
➢ **At the regional scale** → Using SAR imagery (*Kuenzer et al., 2013*)	Low temporal sampling, data availability in L-band
→ Using optical and IR imagery like MODIS (*Frappart et al., 2018*)	Only over regions with few vegetation cover, cloud cover

➢ **What about GNSS-Reflectometry ?**

→ **Only studied at the regional scale**: *Chew et al., 2018; Jensen et al., 2018; Morris et al., 2019; Rodriguez-Alvarez et al., 2019*

→ Monitoring of extreme events (hurricanes, typhoons…)

→ **Threshold methods** that cannot be extended at the global scale

Mapping of CYGNSS reflectivity over land

1. Preprocessing

- Extraction of the DDM peak power
- Subsetting
- CYGNSS flags (ocean mask + quality flags)

2. Coherent reflectivity computation

$$\Gamma_{RL}(\theta_i) = \left(\frac{4\pi}{\lambda}\right)^2 \frac{P_{RL}^{coh}(r_{st} + r_{sr})^2}{P_t G_t G_r}$$

With :

- Γ_{RL} : CYGNSS reflectivity
- P_{RL}^{coh} : DDM peak power
- r_{st} : range from surface to transmitter
- r_{sr} : range from surface to receiver
- $P_t G_t$: GPS EIRP (equivalent isotropically radiated power)
- Gr : antenna gain of the receiver

Signal reflected over

Smooth surface with high SM content or floods	Rough water surface (ocean), dry land…
Coherent reflectivity	**Incoherent reflectivity**

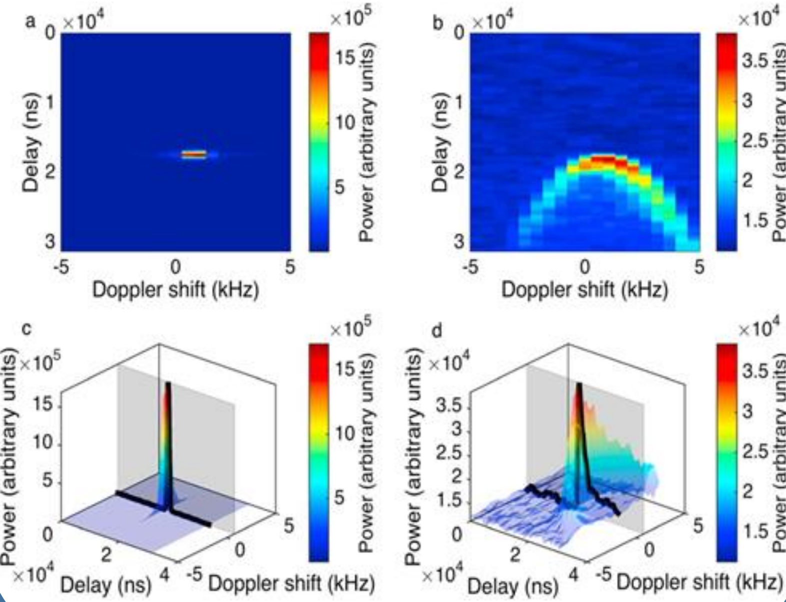

Chew et al. (2016)

Mapping of CYGNSS reflectivity over land

3. Gridding CYGNSS reflectivity

- 0.1°, 7 days grid
- Gaps due to pseudo-random bistatic configuration
- Moving average with Gaussian weighting (1 month)

→ **CYGNSS parameters extracted:**

- Weighted Γ_{mean} and Γ_{std}
- $\Gamma_{90\%}$ (90^{th} percentile)
- Γ_{median} and Γ_{MAD} (median absolute deviation)

→ **Key point:** less observations around the Equator than at higher latitudes

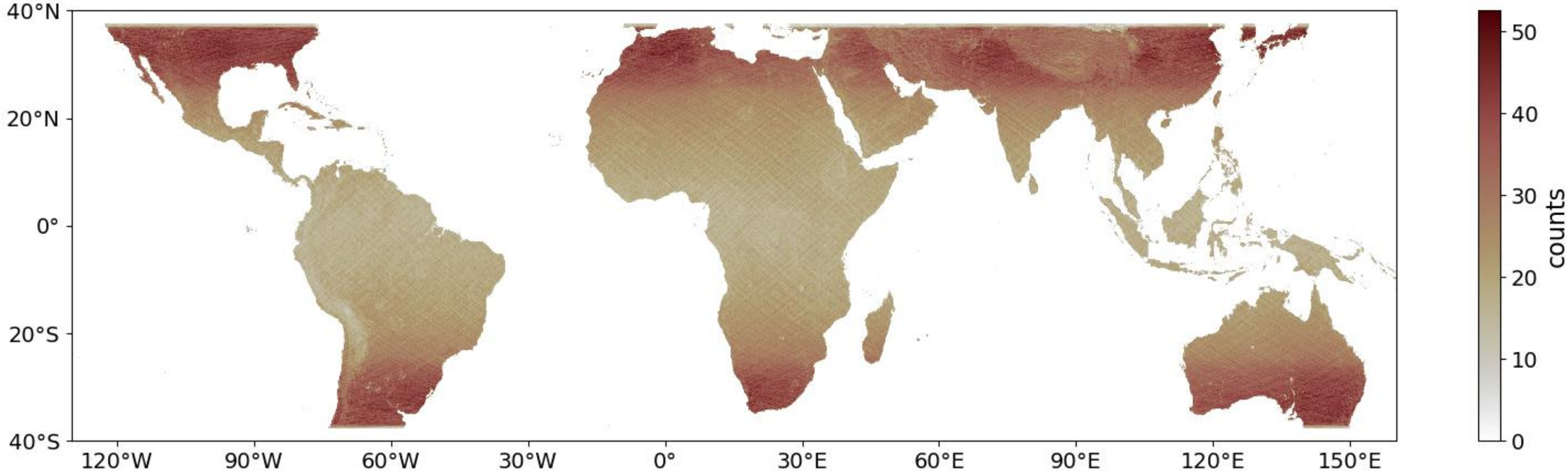

Mean number of observation per pixel in the 0.1°, 7 days grid

Mapping of CYGNSS reflectivity over land

4. Clustering of CYGNSS reflectivity

- K-means clustering with **Dynamic Time Warping (DTW)** similarity measure for **time-series analysis**
- Parameter : $\Delta\Gamma_{90-50} = \Gamma_{90\%} - \Gamma_{median}$
- Time series padding to avoid boundary effect

→ **Key point:** delineation or the major rivers and floodplains at global scale

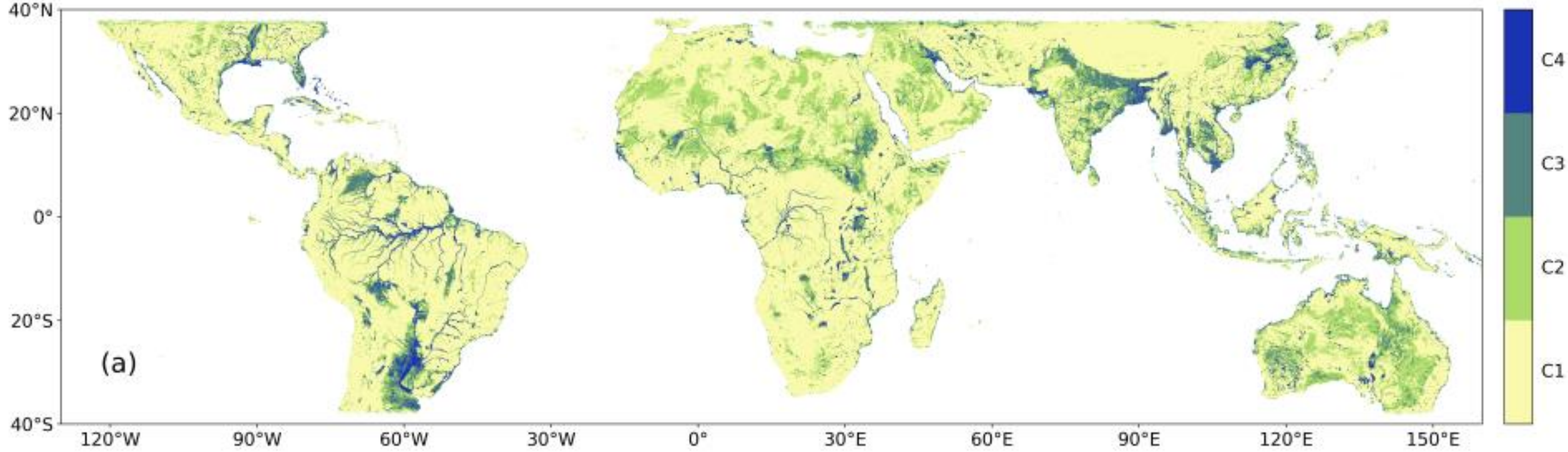

Result of the K-means – DTW clustering of $\Delta\Gamma_{90-50}$. The cluster C1 has the lowest average reflectivity, and the cluster C4 has the highest. From Zeiger et al., 2022, under review.

Extraction of flood patterns

→ **Key point:** very high, ~constant reflectivity for C4. High reflectivity and strong seasonality for C3.

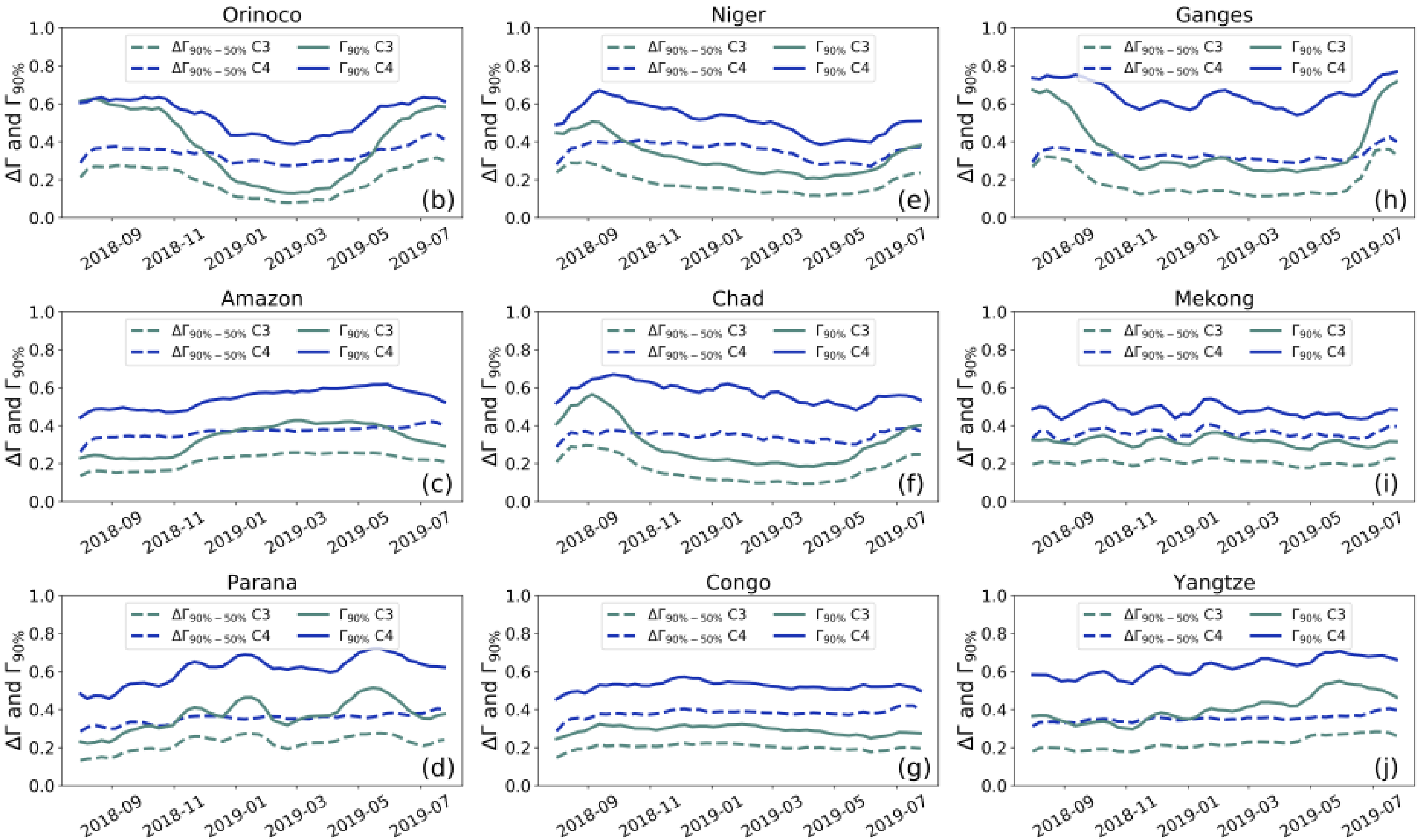

Average time series of reflectivity per basin for cluster C3 and C4. From Zeiger et al., 2022, under review.

Comparison with static inundation maps

→ **Key point:** very high, ~constant reflectivity for C4. High reflectivity and strong seasonality for C3.

$\Gamma_{90\%}$

Clusters

% Water

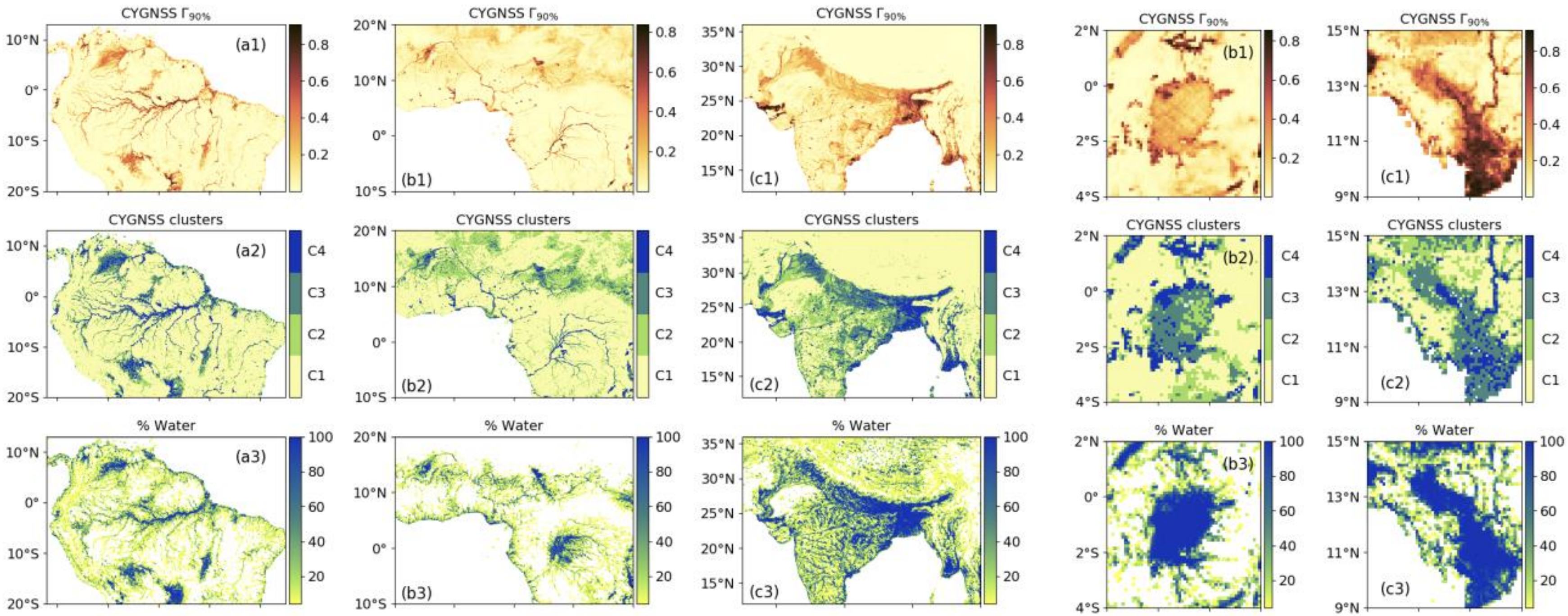

Amazon & Orinoco **Niger, Chad & Congo** **Ganges & Brahmaputra** **Lake Victoria** **Tonle Sap / Delta of Mekong**

Regional Comparison of CYGNSS reflectivity and clusters with the percentage of Regularly Flooded Areas (Tootchi et al., 2019).

From Zeiger et al., 2022, under review.

Comparison with dynamic inundation maps

- **Comparison of CYGNSS reflectivity with GIEMS Surface Water Extent (SWE)**

→ **Key point:** - high correlation (R > 0.8) in most of the major floodplains and irrigated fields.
- lower correlation on coastal areas (limitation of GIEMS), over densely vegetated areas (Cuvette Centrale of Congo), etc.

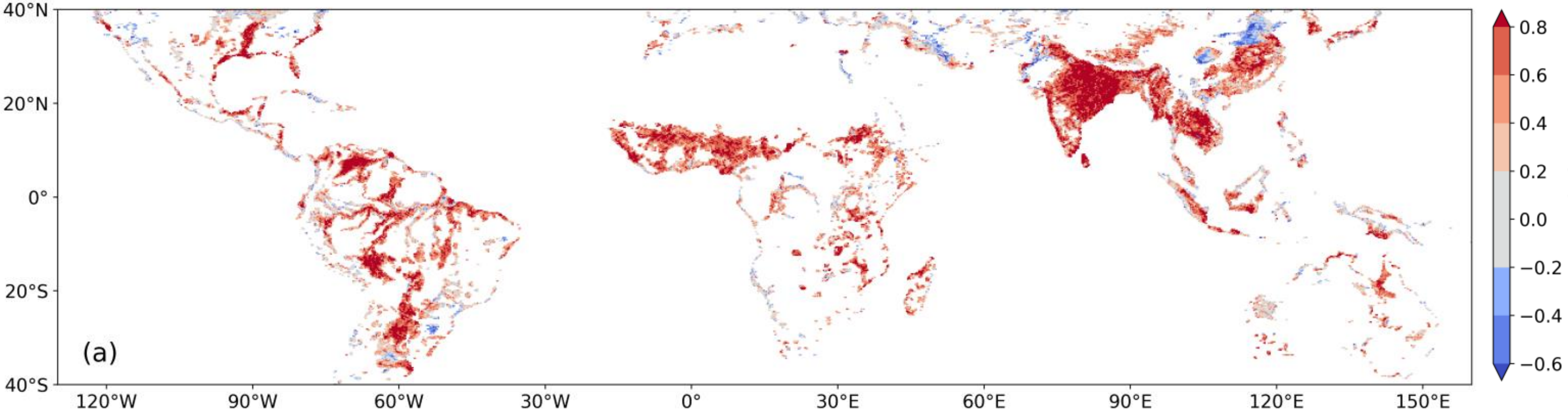

Pixel-by-pixel correlation of CYGNSS reflectivity and GIEMS Surface Water Extent time series.

From Zeiger et al., 2022, under review.

Comparison with dynamic inundation maps

- ➢ **Regional comparison of CYGNSS reflectivity with SWE from MODIS**
  - MODIS SWE extracted using a threshold method (Frappart et al., 2018; Normandin et al., 2018)

→ **Key point:** medium to high correlation over the wetter areas

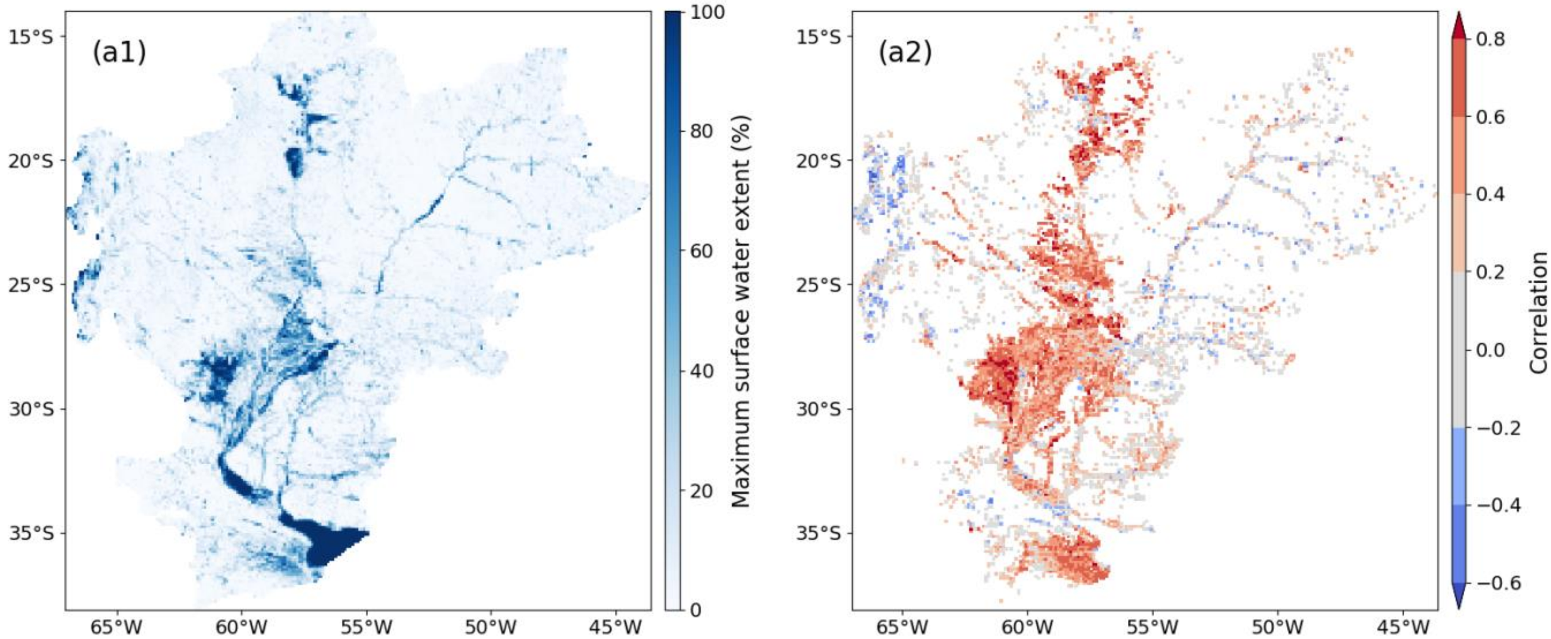

La Plata / Parana basin

Pixel-by-pixel correlation of CYGNSS reflectivity and MODIS Surface Water Extent time series (Frappart et al., 2018).

From Zeiger et al., 2022, under review.

Comparison with dynamic inundation maps

- **Regional comparison of CYGNSS reflectivity with SWE from MODIS**
  - MODIS SWE extracted using a threshold method (Frappart et al., 2018; Normandin et al., 2018)

→ **Key point:** CYGNSS reflectivity correlated to SWE unless the temporal variability of SWE is low

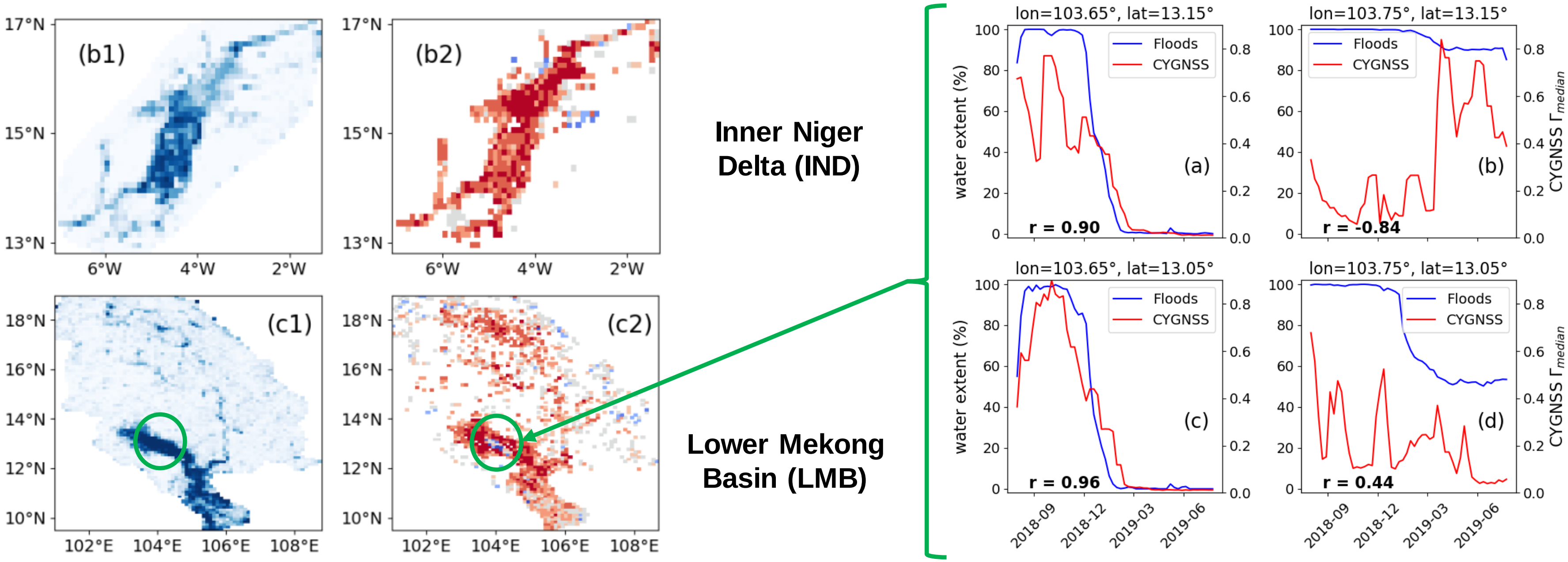

Pixel-by-pixel correlation of CYGNSS reflectivity and MODIS Surface Water Extent time series (Frappart et al., 2018).

Time series of CYGNSS reflectivity and Surface water extent over pixels near the Tonle Sap

From Zeiger et al., 2022, under review.

Toward a dynamic estimation of SWE

- **Relation between CYGNSS $\Gamma_{\mathbf{mean}}$ and SWE from MODIS**

→ Influence of the vegetation and altitude on CYGNSS reflectivity to be removed
→ Binning of CYGNSS, MODIS and GIEMS datasets according to mean values of AGB & DEM in the pixel
→ Linear relationship found in every bin

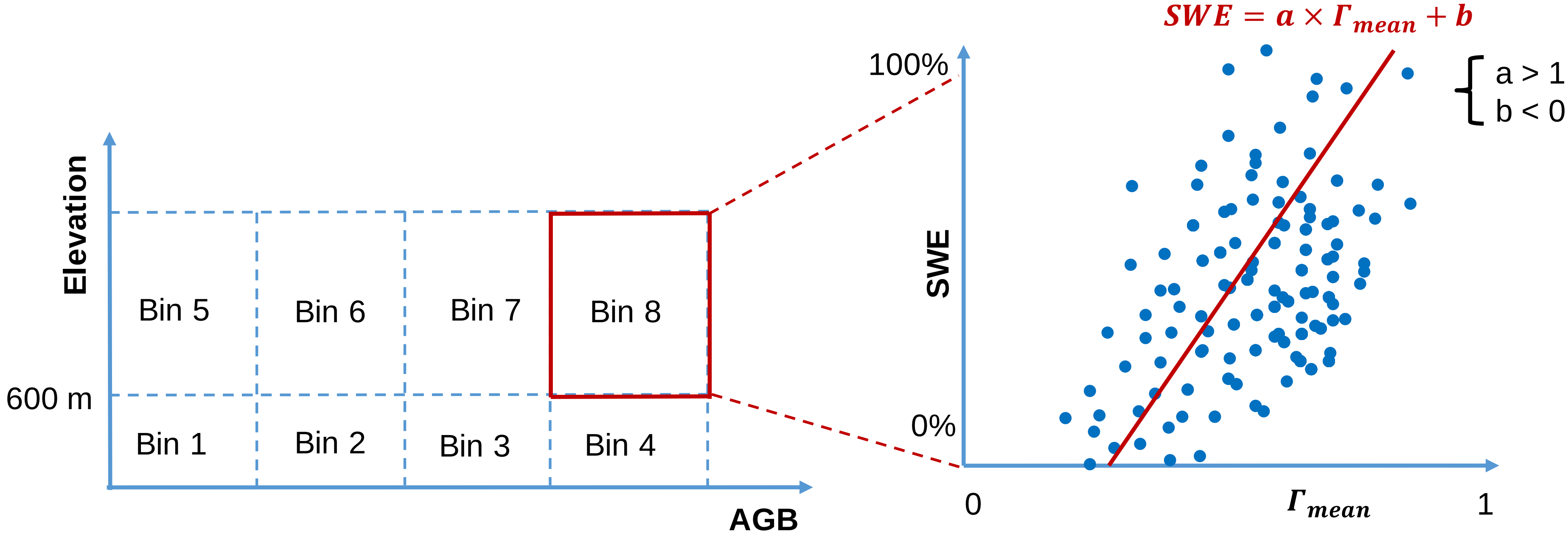

Toward a dynamic estimation of SWE

- **Relation between CYGNSS Γ_{mean} and SWE from MODIS**
  - → **Key point:** clear linear relationship that can be used for regression

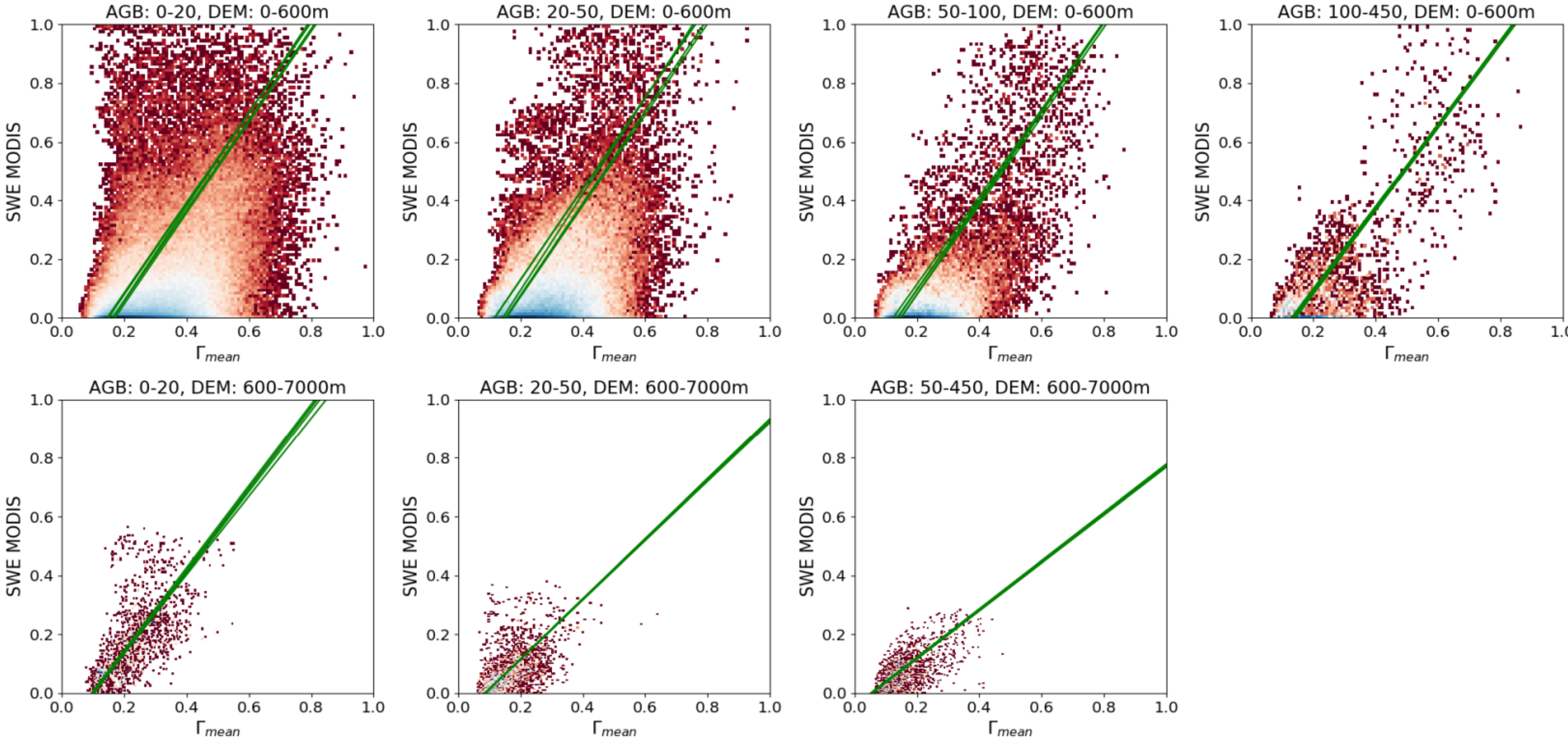

2D histograms of SWE vs. Γ_{mean} for every AGB / DEM bin. The linear curves from a k-fold fit are shown in green.

Toward a dynamic estimation of SWE

- **CYGNSS SWE vs. GIEMS + MODIS**

→ CYGNSS in agreement with MODIS over Niger & Mekong

→ Overestimation of SWE in the Parana → SM ?

→ CYGNSS very lower than GIEMS over equatorial basins (Amazon, Congo) and under high flood regimes (Orinoco, Ganges, Yangtze, Mekong)

→ Underestimation of floods in the Amazon and Congo basins in particular due to vegetation effects

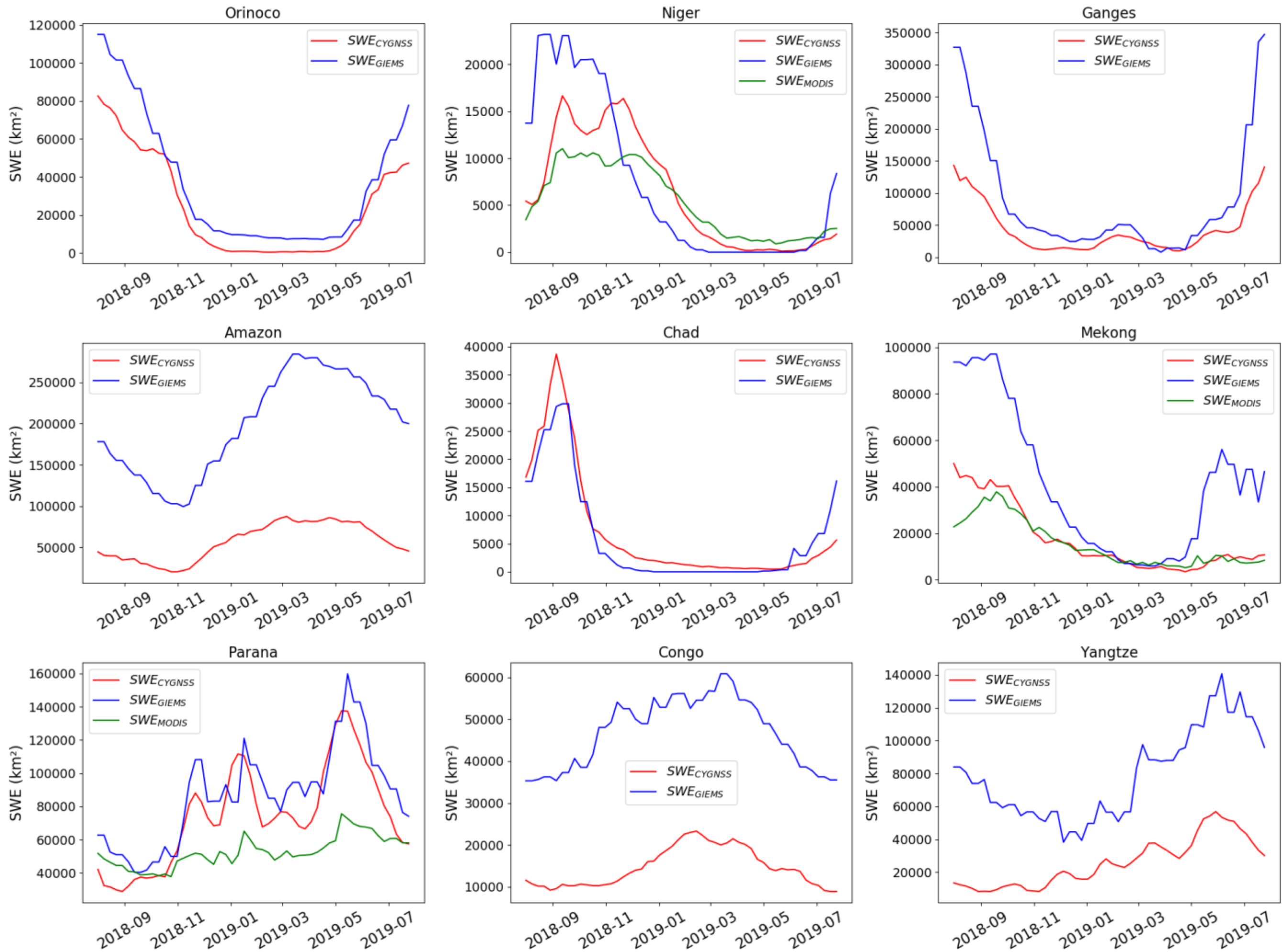

Time series of total SWE from CYGNSS (red), GIEMS (blue) and MODIS (green) per basin

Conclusion

➢ **CYGNSS shows high sensitivity to Surface Water Extent**

→ Detection of the main floodplains and open water bodies using a K-means / DTW clustering
→ Separation of constant and seasonal flood patterns
→ Seasonality of CYGNSS reflectivity agrees with the dynamics of floods (SWE from MODIS or GIEMS)
→ Limitations: dense vegetation, altitude

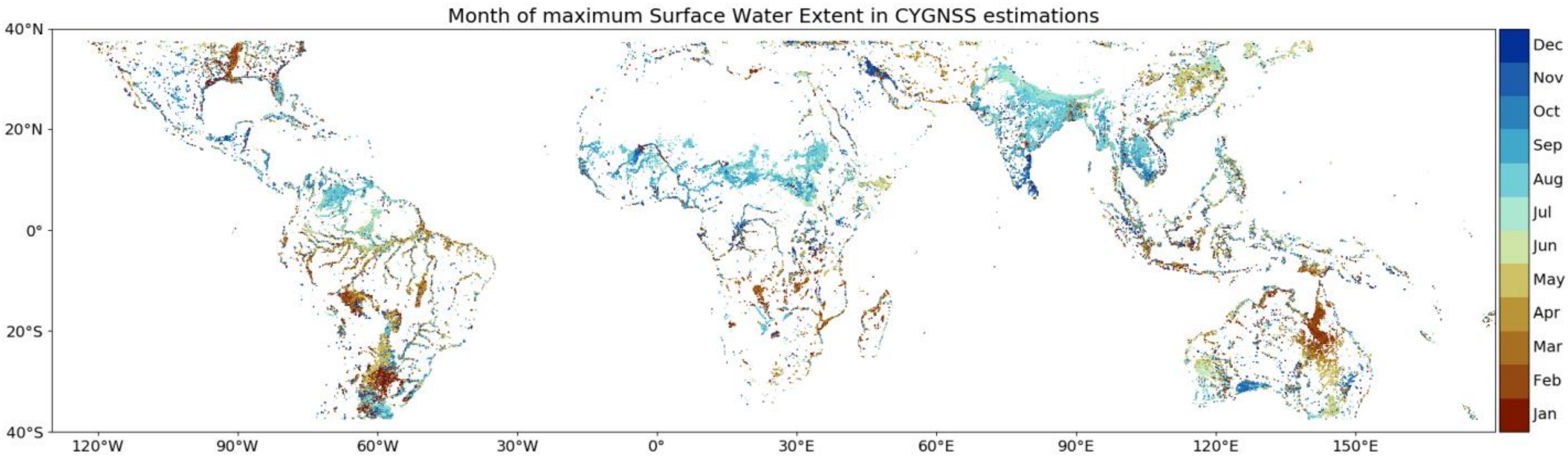

Month of maximum flooded extent in CYGNSS SWE estimation

Conclusion

- **Toward a CYGNSS SWE product (work in progress)**
  - → Linear relationship between CYGNSS reflectivity and MODIS SWE when removing the influence of the vegetation and altitude
  - → Calculation of a 0.1°, 7-day dynamic product of water fraction using CYGNSS in the pan-tropical area
  - → Final product will be available after **correction of the vegetation and SM effects**

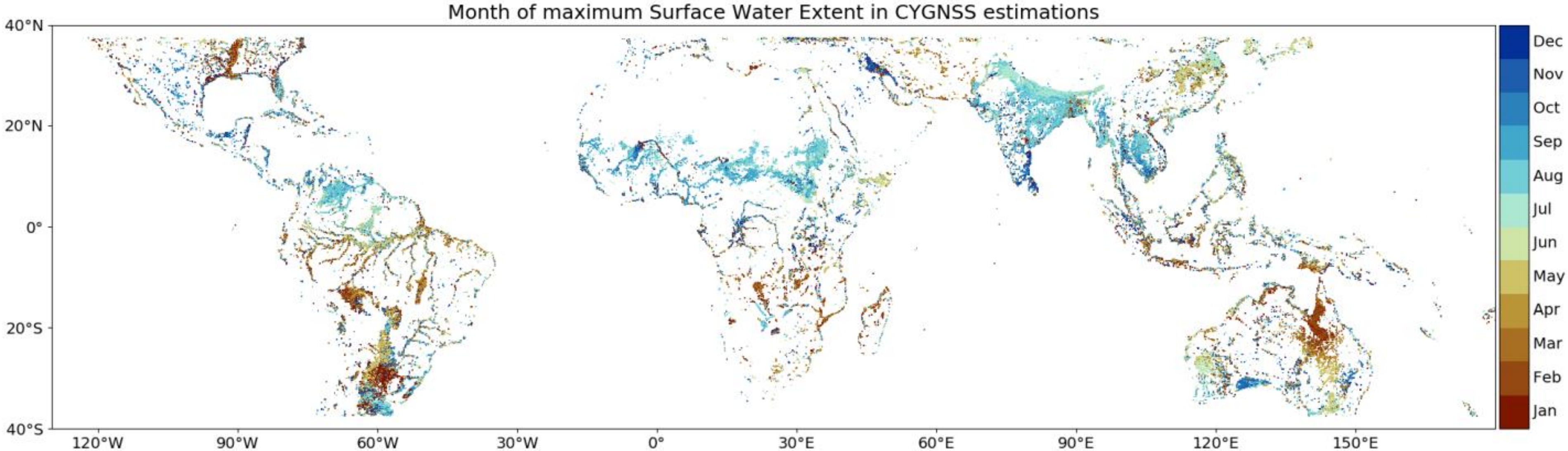

Month of maximum flooded extent in CYGNSS SWE estimation

Thank you for your attention !

Pierre ZEIGER *
Frédéric FRAPPART
José DARROZES

* pierre.zeiger@legos.obs-mip.fr

References:

Chew, C., Reager, J. T., & Small, E. (2018). CYGNSS datamap flood inundation during the 2017 Atlantic hurricane season. *Sci Rep*, 8, 9336

Frappart, F., Biancamaria, S., Normandin, C., *et al*. (2018). Influence of recent climatic events on the surface water storage of the Tonle Sap Lake. *Science of The Total Environment*, 636, 1520–1533.

Jensen, K. & Mcdonald, K. (2019). Surface Water Microwave Product Series Version 3: A Near-Real Time and 25-Year Historical Global Inundated Area Fraction Time Series From Active and Passive Microwave Remote Sensing, *IEEE Geoscience and Remote Sensing Letters*, vol. 16, no. 9, pp. 1402-1406

Kuenzer, C., Guo, H., Huth, J., *et al*. (2013). Flood Mapping and Flood Dynamics of the Mekong Delta: ENVISAT-ASAR-WSM Based Time Series Analyses. *Remote Sensing*, 5, 687–715.

Morris, M., Chew, C., Reager, J. T., *et al.* (2019). A novel approach to monitoring wetland dynamics using CYGNSS: Everglades case study. *Remote Sensing of Environment*, 233, 111417

Pekel, J.-F., Cottam, A., Gorelick, N., & Belward, A. S. (2016). High-resolution mapping of global surface water and its long-term changes. *Nature*, 540, 418–422.

Prigent, C., Jimenez, C., & Bousquet, P. (2020). Satellite-Derived Global Surface Water Extent and Dynamics Over the Last 25 Years (GIEMS-2). *J. Geophys. Res. Atmos*., 125.

Rodriguez-Alvarez, N., Podest, E., Jensen, K., & McDonald, K. C. (2019). Classifying Inundation in a Tropical Wetlands Complex with GNSS-R. *Remote Sensing*, 11, 1053

Tootchi, A., Jost, A., & Ducharne, A. (2019). Multi-source global wetland maps combining surface water imagery and groundwater constraints. *Earth Syst. Sci. Data*, 11, 189–220.

Zeiger, P., Frappart, F., Darrozes, J., Prigent, C., & Jiménez, C. (2022). Analysis of CYGNSS coherent reflectivity over land for the characterization of pan-tropical inundation dynamics. *Submitted to Remote Sensing of Environment, under review*.